PCCP

Antimony and bismuth oxide cluster ions

Jörg Opitz-Coutureau, André Fielicke, Bernhard Kaiser and Klaus Rademann*

Walther-Nernst-Institut für Physikalische und Theoretische Chemie der Humboldt-Universität zu Berlin, Bunsenstrasse 1, D-10117 Berlin, Germany. E-mail: ehlers@chemie.hu-berlin.de

Received 3rd April 2001, Accepted 31st May 2001
First published as an Advance Article on the web 2nd July 2001

The formation of charged antimony and bismuth oxide clusters in a pulsed arc cluster ion source (PACIS) has been studied with time-of-flight mass spectrometric techniques. We compare series of antimony and bismuth oxide cluster anions with their known cationic counterparts. The anionic series $(M_2O_3)_nMO_2^-$ and $(M_2O_3)_nO_2^-$ have been predicted proceeding from the known cationic series $(M_2O_3)_nMO^+$ and $(M_2O_3)_nO^+$ by adding O^{2-} and have been experimentally established. All these series contain the metal atoms (M = Sb or Bi) in the formal oxidation state +3. However, only in the case of antimony, oxygen rich oxide clusters appear, that can be explained with a gradual transition in the oxidation number from +3 to +5 of single antimony atoms in the cluster. To estimate the influence of the special oxide formation conditions comparative investigations with the PACIS and a laser vaporisation cluster source have been carried out for bismuth oxide cations. The similar oxide cluster distributions at comparable oxygen availability display clearly that the special thermodynamical stability of the discussed magic clusters is the significant driving force for their formation.

Introduction

One focal point of studying gaseous clusters is their structure, since all physical characteristics and the chemical behaviour are closely related to it.[1,2] The size-depending evolution of properties[3] makes the cluster a tool to investigate bulk growth processes. However, the frequently used experimental methods for determining three-dimensional structures are usually not applicable to cluster systems. One main problem is the commonly low particle density that prevents the usage of diffraction or most spectroscopic techniques. Suitable solutions are advanced quantum chemical computations, which excellently complement the rare experimental structure research. But especially for large and heavier clusters an enormous computational expenditure is necessary and very often many isomers are to be considered. For the topology of covalent systems of mesoscopic size the method of valance electron counting has been established to describe the skeleton of the electron pair bonds.[4,5] Hence, first indications for the clusters' stability can be obtained. These electron counting rules still help to fill the gap between the characterisation of molecule-like small clusters and the structure of the bulk phase. Nevertheless, by applying these concepts, only the topology of a cluster and not directly the structure is indicated. A common experimental method to study aspects of stability and topology of clusters utilises the evolution of "magic" series patterns extracted from mass spectra. Insights into stability principles and structures are prerequisites for understanding the chemical behaviour of small clusters.[6–14]

The oxides of group V elements are suitable tools for studying structural transitions in clusters, since they show already in the solid phase an interesting polymorphic behaviour. This polymorphism is accompanied by altering connectivities, which are reflected even in the stability principles of the polynuclear oxides in the gas phase.[15] For instance, at room temperature the stable solid phase of Sb_2O_3 is the cubic senarmontite, which contains the Sb_4O_6 molecule,[16] whereas the high temperature orthorhombic phase valentinite has a polymeric sheet structure built up from eight-membered Sb_4O_4 rings.[17] The existence of Sb_4O_6 molecules in the gas phase of antimony(III) oxide is well known since the measurement of the vapour density by Meyer and Meyer in 1879[18] and the tetrahedral structure has been proven by electron diffraction.[19,20] This dimer $(Sb_2O_3)_2$ is the first member of the polymeric cluster series $(Sb_2O_3)_n$ that has been actually produced by laser vaporisation[21] and gas aggregation techniques.[22,23] Cationic clusters of this stoichiometry have been made with a pulsed arc discharge cluster ion source (PACIS),[24,25] but apparently cluster cations with the stoichiometry $(Sb_2O_3)_nSbO^+$ are found to be more intense, because of their high stability. These cations have been observed earlier by laser-induced vaporisation of different solid antimony oxides phases.[26] Structural similarities between the clusters $(Sb_2O_3)_nSbO^+$ and the connectivity of the sheets in the orthorhombic antimony oxide phase valentinite have been emphasized by Reddy and Jena.[15] An oxide of antimony(V) is known but it is structurally less well characterised. Generally, structural motives in antimony(V) oxides are distorted $Sb^{+V}O_6$ octahedrons, which also appear in the mixed valence oxide Sb_2O_4. Until now, pure oxide clusters with all antimony in +5 oxidation state have not been characterised. A transition in the oxidation state from +3 to +5 of a few antimony atoms in oxide clusters has been observed especially for larger clusters.[21,25] In these clusters the antimony(V) atoms are fourfold coordinated, in contrast to the Sb-coordination in the solid oxides. The solid oxides of bismuth(III) have three-dimensional structures,[27] which are less well described by molecular concepts. In contrast to the other pnicogens (except nitrogen), a cubic oxide modification containing the Bi_4O_6 molecule does not exist. Also, stable oxides of bismuth(V) are not known. Remarkably, several polynuclear oxygen bridged oxo-, hydroxo- and alkoxo-clusters of Bi^{+III} were already synthesised and structurally characterised several decades ago in solution and solid state phases.[28–30] Compounds of this type

 DOI: 10.1039/b103009b

have been recently discussed as precursors for high T_C superconductors *via* sol–gel processes. The high temperature phase equilibria in the bismuth–oxygen system as well as Knudsen cell vaporisation studies leading to small polynuclear bismuth oxide molecules have been discussed in detail by Oniyama and Wahlbeck.[31] Furthermore, investigations of gas phase bismuth oxide clusters have been reported in connection with the corresponding antimony oxide clusters.[21,22,32]

Hitherto, experimental work on group V oxide clusters has been mainly focussed on neutral and positively charged species. The mass spectra of the cationic antimony and bismuth oxide clusters reveal magic number series $(M_2O_3)_nMO^+$ and $(M_2O_3)_n^+$ which are similar for M = Sb or Bi.[21,22,24,25,33] The remarkable intensity of the oxide cations $(M_2O_3)_nMO^+$ has been explained by straightforward valence bond arguments using simple electron counting rules.[22,24] In contrast, little is known about the anionic oxide clusters. Bismuth oxide anions containing only two or three bismuth atoms have been presented by France *et al.*[21] and the influence of the charge on electronic structure effects has been emphasized, but this could not be proven hitherto for larger clusters and no anionic series have been formulated.

Here, we report a detailed comparison of positively and negatively charged antimony and bismuth oxide cluster ions. The cluster distributions are produced under similar conditions in a pulsed arc cluster ion source (PACIS). The study is focussed on mass spectrometric investigations of oxide clusters produced in plasma reactions of oxygen and antimony or bismuth, respectively. Insights into stability principles have been obtained by monitoring the cluster distributions as the formation conditions are changed. For the bismuth oxide cluster cations these results have been confirmed by complementary experiments using a laser vaporisation cluster source (LVS).

Experimental

PACIS

For cluster generation and mass spectrometric analysis we use a three stage differentially pumped molecular beam apparatus consisting of the source chamber, the acceleration chamber and the detection chamber. The flight path of the cluster ions passes a skimmer with a 3 mm opening between the first two chambers and a simple hole arrangement with a 6 mm opening between the last two chambers. The pulsed arc cluster ion source (PACIS)[34,35] (see Fig. 1) can be positioned in three dimensions in front of the skimmer [Fig. 1 D] to achieve optimal cluster signal. The maximum displacement is 10 mm in *X* and *Y* and 50 mm in the *Z*-direction, which is along the beam axis. The body B of the source is made of machineable glass ceramics (MARCOR™), which electrically isolates the electrodes. Gas valve A and nozzle extender C are attached to this body. The 8 mm diameter cathode is vacuum melted either from antimony shots (Johnson–Matthey, purity 99.999%) or bismuth needles (Johnson–Matthey, 99.999%). The anode is made of molybdenum (Goodfellow, 99.9%). The seed gas pulse of a typical duration of 400 μs is applied by a pulsed electromagnetic valve (General Valve series #9) [Fig. 1 A]. Cluster ions are produced by an arc discharge between the two electrodes, which leads to erosion of the cathode. Pure antimony and bismuth cluster ions of both charge states are obtained with pure helium (Messer–Griesheim, 99.9999%) as seed gas. Oxide clusters are formed when oxygen is premixed to the seed gas. Commercially available gas premixtures (Messer–Griesheim, He 99.999%, O_2 99.995%) were used for this reason. The influence of different oxygen partial pressures in the seed gas on the growth of oxide clusters is studied by using gas mixtures of 0.1%, 1.0% and 10.0% oxygen content. Cluster formation takes place by multiple collisions in the plasma. Collisional cooling in the helium gas flow through the nozzle extender 'C' as well as the adiabatic expansion into the vacuum leads to supersaturation and further cluster growth. During the operation the whole source is kept at a constant temperature of 10 °C by two water-cooled shrouds [Fig. 1 E].

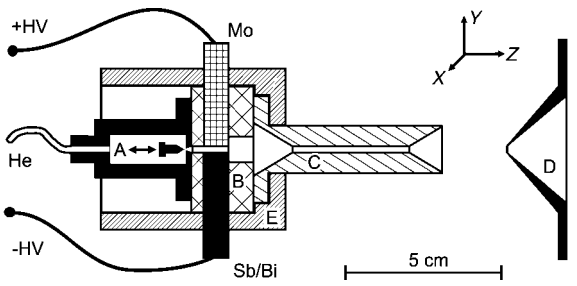

Fig. 1 Schematic drawing of the pulsed arc cluster ion source: (A) Pulsed electromagnetic valve, (Sb/Bi) antimony or bismuth cathode rod, (Mo) molybdenum anode rod, (B) body of the source made of MACOR™ glass ceramics, (C) nozzle extender, (D) skimmer, (E) cooling shrouds.

After entering the second chamber the cluster ions are accelerated and focused by an on-axis Wiley–McLaren type time-of-flight mass spectrometer, which has been described previously.[36] In the third chamber, an on-axis reflectron arrangement is used to enhance the mass resolution of the detection system. All high voltages are applied to the acceleration plates using solid state high voltage switches (Behlke). Cations are detected by a MCP-detector whereas the anions are detected by a channeltron-detector, which is floated at high positive potential. Time-of-flight mass spectra were recorded typically by averaging over 4000 arc discharges. During the experiment the typical pressure in the acceleration and detection chambers is about 1×10^{-8} mbar.

Reactive laser vaporisation

The formation of bismuth oxide cluster cations has also been studied with a second molecular beam machine equipped with a laser vaporisation cluster source with continuous flowing carrier gas. The construction of this apparatus has been described previously.[13] Briefly, it consists of three differentially pumped vacuum chambers. The first chamber contains the cluster source. The second pressure stage is separated from the first by a skimmer with a 2 mm orifice and from the third by a 5 mm aperture. The last chamber contains a Wiley–McLaren type time-of-flight mass spectrometer,[37] wherein the ions are accelerated perpendicular to the original direction of the molecular beam. An electrostatic lens and deflector plates guide the ions towards a modified Daly detector "Even-Cup".[38,39] The spectra were recorded with a digital oscilloscope (Lecroy 9350 CM) and averaged over 1000 single shot spectra.

The assembly of the laser vaporisation source (LVS) is shown in Fig. 2. The body B of the source contains a rotating metal rod (∅ 5 mm) from which the material is vaporised by

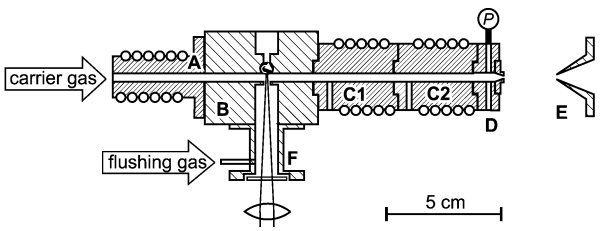

Fig. 2 Set-up of the laser vaporisation cluster source: (B) source body with rotating target rod; (A), (C1), and (C2) copper extenders; (D) nozzle part with attached pressure sensor; (E) skimmer; (F) laser window socket.

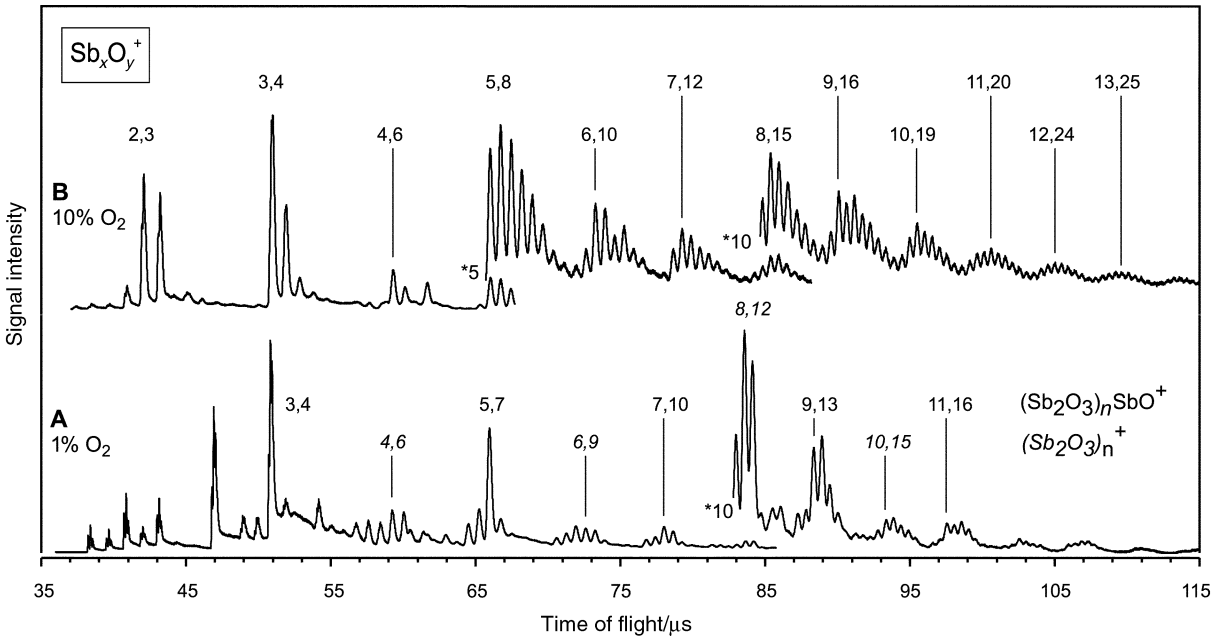

Fig. 3 Time-of-flight mass spectra of antimony oxide cluster cations at different oxygen contents in the seed gas: A 1% and B 10% O_2 (4.5) in He (5.0). The formation of two stable series of antimony oxides $Sb_xO_y^+$ is observed at 1% O_2 in the seed gas (A). The stoichiometry of the series and their members are indicated. The mass spectra at 10% O_2 contain nearly exclusively higher oxidised antimony oxides (B). The marks indicate the most prominent clusters in the groups evolved from the series depicted in A.

the focussed beam of the second harmonic of a pulsed Nd : YAG laser (Continuum PL 6030) with a typical laser power of 5 mJ per pulse. The vaporised material forms a plasma that is carried through a channel of 4 mm diameter by a stream of helium with added oxygen. A small amount of the gas mixture is admitted in the extender F near the laser window to prevent covering. The plasma is cooled in the gas flow and clusters are formed. The source body B is extended up and downstream by the segments A, C1 and C2 made from copper. A provides the carrier gas socket, whereas C1 and C2 have reactive gas inlets to study cluster reactions. The gas pressure in the channel is measured with a capacitance pressure sensor near the 2 mm conical nozzle. Under working conditions, the pressure is in the order of 30 mbar corresponding to a flow up to 5000 sccm.

Results

Antimony oxide cations

Fig. 3A and Fig 3B show antimony oxide mass spectra obtained by using a PACIS operated with oxygen concentrations of 1% and 10% in the helium seed gas. These data are in agreement with the known mass distributions[21,25] containing the series $(Sb_2O_3)_nSbO^+$ and $(Sb_2O_3)_n^+$. Most prominent peaks in spectrum A are assigned to $Sb_3O_4^+$, $Sb_5O_7^+$, $Sb_7O_{10}^+$ for the first series and $Sb_4O_6^+$, $Sb_6O_9^+$, $Sb_8O_{12}^+$ for the second one, respectively. At 10% O_2 the mass spectra display mainly signals of highly oxygenated clusters. Therefore, if the oxygen content in the seed gas is increased from 1% to 10%, the group maxima are shifted, for instance, from

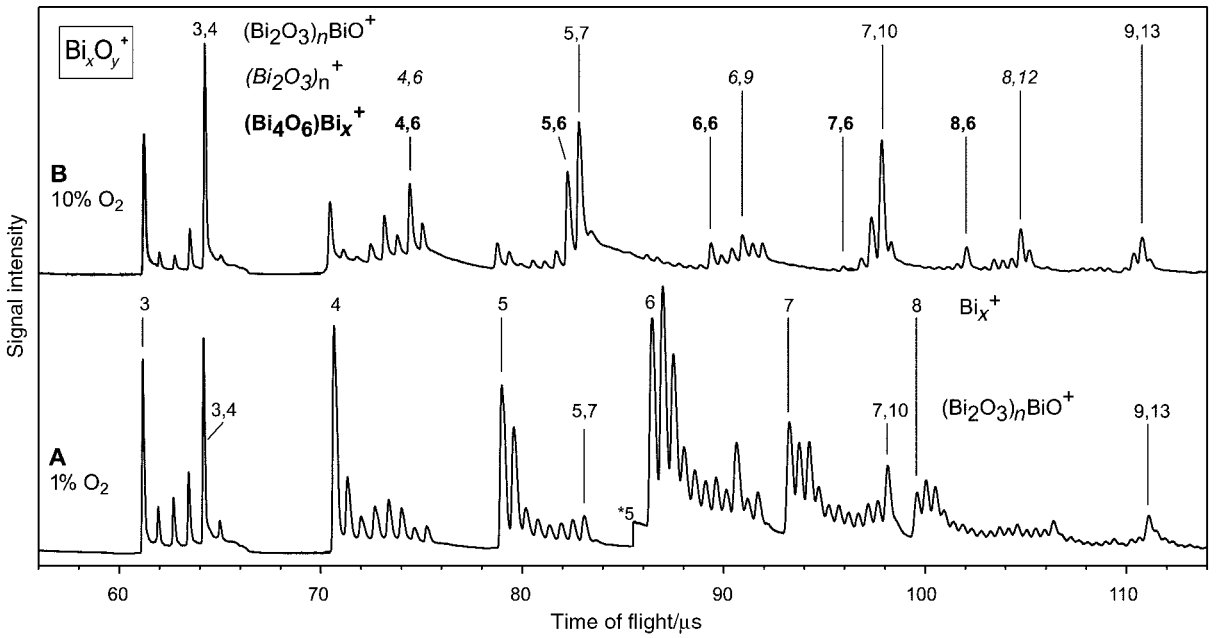

Fig. 4 Time-of-flight mass spectra of bismuth oxide cluster cations at 1% and 10% oxygen concentration in the seed gas. B: Thermodynamically stable bismuth oxide cluster cations dominate the mass spectrum and three series have been identified.

$Sb_5O_7^+$ to $Sb_5O_8^+$ or from $Sb_7O_{10}^+$ to $Sb_7O_{12}^+$. The cationic spectra have been reproduced in order to compare them with the newly investigated anionic systems, *vide infra*.

Bismuth oxide cations

Time-of-flight mass distributions of bismuth oxide cluster cations produced with the PACIS at 1% O_2 and 10% O_2 are displayed in Fig. 4A and B. The dominating feature at 1% O_2 addition is still the existence of pure bismuth cluster cations Bi_x^+ ($3 \leqslant x \leqslant 8$). The detected signals of oxide clusters already show certain structures. $Bi_3O_4^+$ is the most intense oxide cluster of all. $Bi_7O_{10}^+$ and $Bi_9O_{13}^+$ show higher intensities than their neighbours. The peculiarity of these clusters becomes clearer if the oxygen concentration is increased. Again, at 10% O_2 the most prominent signals are attributed to the clusters $Bi_3O_4^+$, $Bi_5O_7^+$, $Bi_7O_{10}^+$ and $Bi_9O_{13}^+$ belonging to the series $(Bi_2O_3)_nBiO^+$. This "magic number" series can be clearly observed up to $n = 32$. Other remarkable intense clusters $Bi_4O_6^+$, $Bi_6O_9^+$ and $Bi_8O_{12}^+$ are members of the series $(Bi_2O_3)_n^+$ (observed up to $n = 33$).

A third series of clusters $(Bi_4O_6)Bi_x^+$ ($0 \leqslant x \leqslant 4$) is found with the constituents $Bi_4O_6^+$, $Bi_5O_6^+$, $Bi_6O_6^+$, $Bi_7O_6^+$ and $Bi_8O_6^+$. This series becomes more evident in the oxide distribution obtained by laser vaporisation. Fig. 5 displays a mass spectrum of bismuth oxide cations produced with the laser vaporisation cluster source by adding 10% of molecular oxygen to the seed gas. Remarkably, this oxide distribution is very similar to that achieved with the PACIS. In addition, signals of clusters with one extra oxygen atom are particularly strong, corresponding to the series $(Bi_2O_3)_nO^+$, which has not been recognised heretofore in the literature.

Bismuth oxide anions

In Fig. 6 we present a broad range time-of-flight mass spectrum of the negatively charged bismuth oxide cluster ions $Bi_xO_y^-$ up to $x = 10$ formed in the PACIS at 1% oxygen added to the seed gas. Similar to the cationic mass spectra the formation of well-structured anionic oxide cluster groups has been observed. Each group has a distinct number of metal atoms and a varying number of oxygen atoms. An analysis of these groups shows the preferred formation of certain cluster series, which are different for cations and anions. For instance, $Bi_3O_5^-$, $Bi_5O_8^-$, $Bi_7O_{11}^-$ belong to the series $(Bi_2O_3)_nBiO_2^-$, whereas $Bi_2O_4^-$, $Bi_4O_7^-$, $Bi_6O_{10}^-$ are members of $(Bi_2O_3)_nO^-$ and $Bi_2O_5^-$, $Bi_4O_8^-$, $Bi_6O_{11}^-$ belong to the series $(Bi_2O_3)_nO_2^-$. Compared to cationic systems the mass spectra are obtained at oxygen concentrations that are an order of magnitude lower. However, the signals are strongly depleted at 10% O_2.

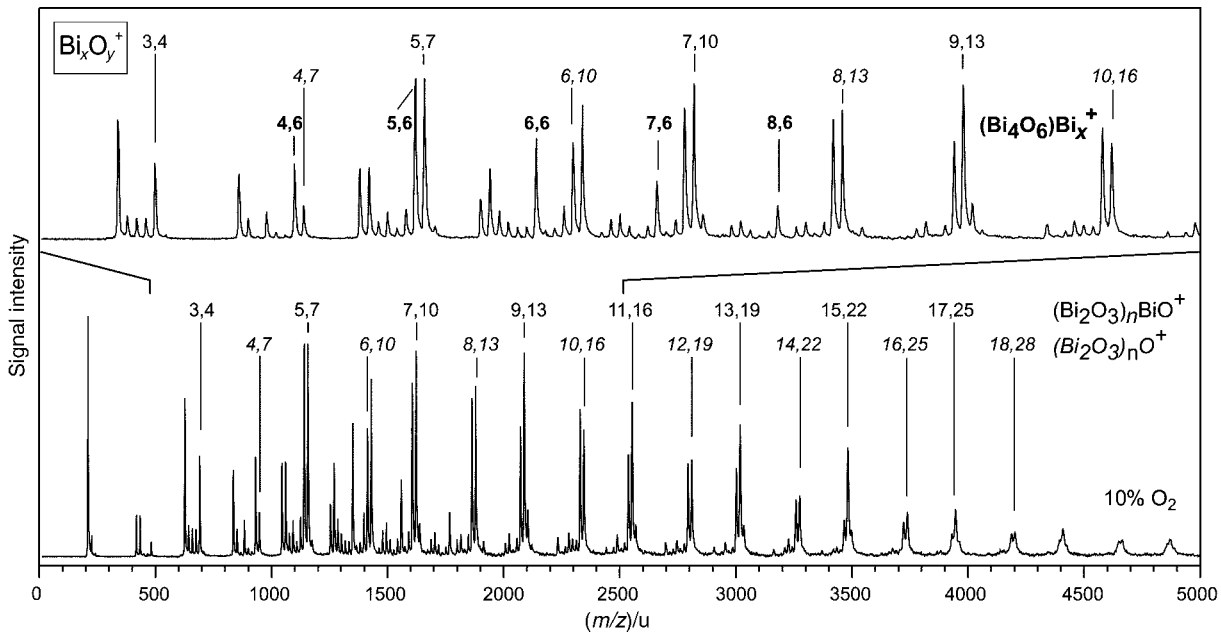

Fig. 5 Cationic cluster distributions produced with the laser vaporisation source (LVS). 10% oxygen in the seed gas leads to the formation of prominent series for $(Bi_2O_3)_nBiO^+$, $(Bi_2O_3)_nO^+$ and $(Bi_2O_3)_n^+$ (not marked), which dominate the spectrum especially for the larger clusters. The composition of the oxide cations $Bi_xO_y^+$ is given as couples *x,y*. The upper trace shows the stretched mass range 500–2500 u.

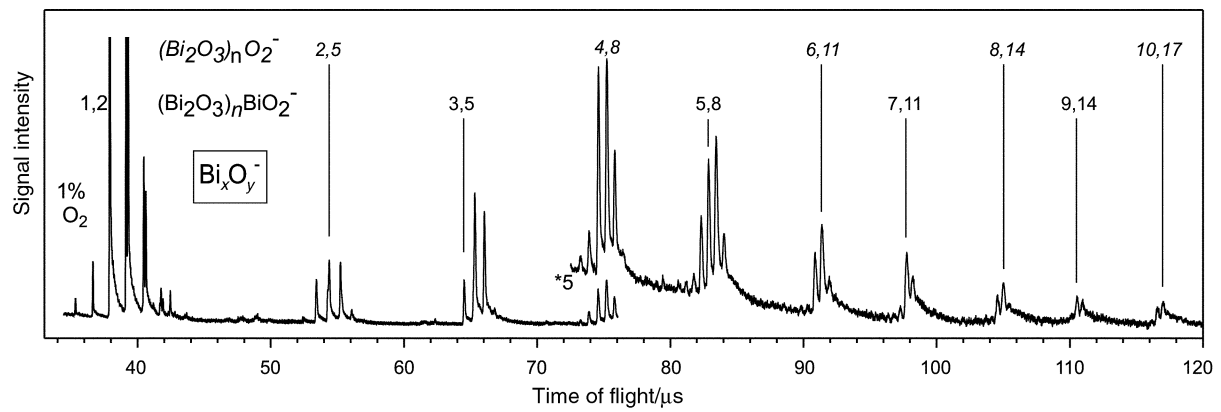

Fig. 6 Time-of-flight mass spectra of bismuth oxide anions 1% oxygen content in the seed gas. Thermodynamically controlled oxide cluster growth leads to the formation of thermodynamically stable series: $(Bi_2O_3)_nO_2^-$ ($1 \leqslant n \leqslant 5$) and $(Bi_2O_3)_nBiO_2^-$ ($1 \leqslant n \leqslant 4$).

Antimony oxide anions

Time-of-flight mass spectra of antimony oxide cluster anions obtained by using the PACIS with 1% and 10% O_2 are shown in Fig. 7. Again, the mass spectra are structured into group patterns, which differ characteristically from the cationic oxide distributions. $Sb_3O_5^-$ and $Sb_5O_8^-$ are very intense oxides at 1% O_2. They belong to the series $(Sb_2O_3)_nSbO_2^-$ with $n = 1$ and $n = 2$, respectively. Further, but less pronounced members of this series are $Sb_7O_{11}^-$ and $Sb_9O_{14}^-$. Stronger signals are observed next to these peaks: Here $Sb_7O_{12}^-$ and $Sb_9O_{15}^-$ establish a new series $(Sb_2O_3)_nSbO_3^-$. Each of these clusters contains already one antimony atom with an oxidation state that has changed from +3 to +5. Another series of clusters following the building principle $(Sb_2O_3)_nO_2^-$ ($1 \leqslant n \leqslant 5$) is marked in Fig. 7A. For $n = 3$, 4 and 5 these clusters are the most intense ones in their groups. The clusters $Sb_2O_4^-$ and $Sb_4O_7^-$ [members of $(Sb_2O_3)_nO^-$] dominate the corresponding groups for $n = 1$ and $n = 2$. If the oxygen concentration in the seed gas is increased to 10%, a general transition to oxygen rich clusters has been observed. Typical compositions are described by the formulae $(Sb_2O_5)_nSbO_2^-$ and $(Sb_2O_5)_n(Sb_2O_4)^-$. Especially for clusters with more than four antimony atoms broad oxide cluster distributions have been found without dominating peaks.

Discussion

Antimony oxide cations

Here we discuss trends in the mass spectrometrically observed oxide cluster series in relation to their metal oxidation state, topology, and stability. Electron counting has been used previously as a simple method to describe the electronic structure of some cationic antimony and bismuth oxide clusters.[22,24] In this scheme it is assumed that all oxygen atoms are in a −2 and the metal atoms are in a +3 oxidation state. For the series $(M_2O_3)_nMO^+$ formal charge counting assigns to the metal $(2 \times 3n + 3)$ positive charges and $(3 \times 2n + 2)$ negative charges to the oxygen atoms. This procedure gives the total charge of the cluster of +1. The second series $(M_2O_3)_n^+$ yields $+(2 \times 3n)$ for M and $-(3 \times 2n)$ for O. The total cluster charge of +1 results in a vacancy of 1 electron with respect to the assigned oxidation numbers.

Extensive *ab initio* quantum chemistry calculations have been performed previously to obtain information about the structure and general building principles for antimony oxide clusters up to $Sb_{13}O_{20}^+$.[25] A common feature of all calculated structures is the formation of a maximum number of Sb–O bonds rather than allowing for Sb–Sb and O–O bonds. Both series $(Sb_2O_3)_nSbO^+$ and $(Sb_2O_3)_n^+$ discussed here were the subject of these theoretical investigations. The calculations corroborated that in these cationic series, except for a defect centre all antimony atoms are trivalent and all oxygen atoms divalent. In the series $(Sb_2O_3)_nSbO^+$ an additional bond to a trivalent oxygen atom avoids an open valence. In the second series $(Sb_2O_3)_n^+$ the unpaired electron in the ionised cage is mainly localised at an antimony atom and to a smaller extent at the three next oxygen atoms. This series meets exactly the stoichiometry of the bulk phase antimony(III) oxide.

A method to present processed mass spectral data are correlation diagrams for the composition of binary compound clusters. In Sb/O-correlation diagrams, the number of the oxygen atoms y in a cluster Sb_xO_y with a certain number of antimony atoms x is plotted for the three most intense clusters of each group. This process leads to enriched information about favoured cluster compositions and trends, in particular, which are not obvious in the raw mass spectra. The Sb/O-correlation diagram for 1% O_2 in the seed gas [Fig. 8] reveals clearly the tendency to form predominantly stoichiometric antimony(III) oxides under this condition: The slope of the points reflects an average oxygen/antimony ratio of 3/2. The lines represent the O/Sb ratio of pure +3 or +5 oxides, respectively.

At high oxygen concentration clusters are observed with one or two additional oxygen atoms following the series $(Sb_2O_3)_nSbO_2^+$ and $(Sb_2O_3)_nSbO_3^+$ (see Fig. 3B). They have been reported previously and their structures have been calculated, too.[25] The calculations reveal that extra oxygen atoms

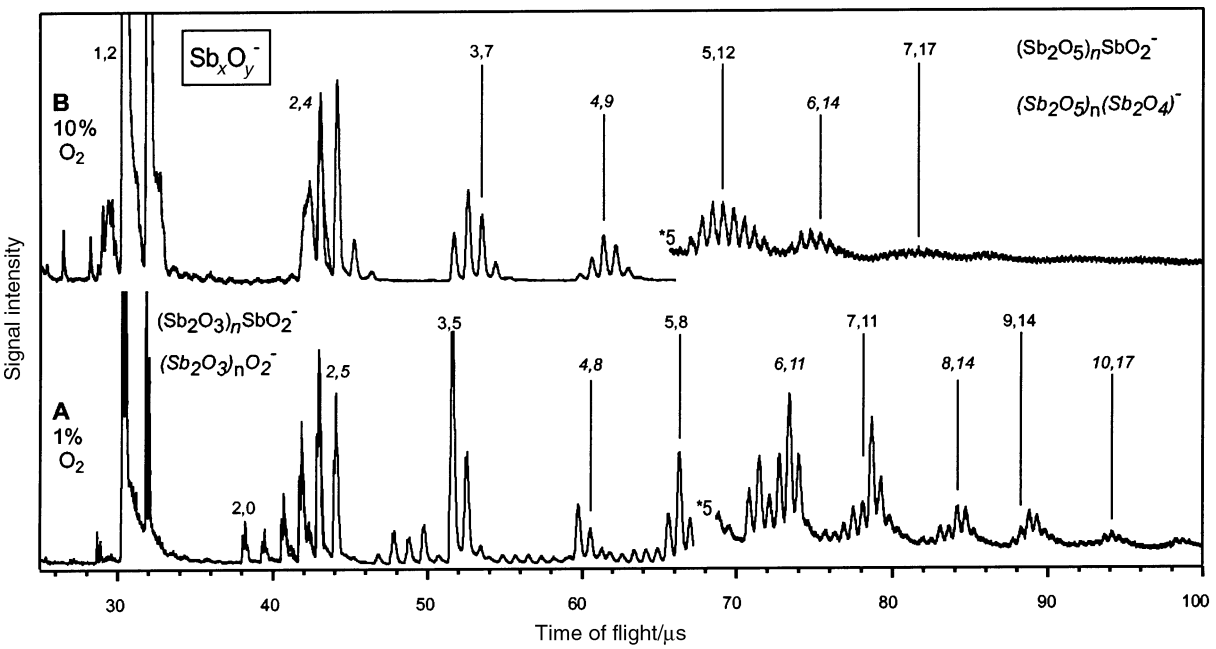

Fig. 7 Time-of-flight mass spectra of antimony oxide anions at two different oxygen concentrations in the seed gas: A 1% and B 10% O_2 in He. At 1% O_2 two series dominate the spectrum where all antimony atoms are in +3 oxidation state. The mass spectrum at 10% O_2 contains nearly exclusively higher oxidised clusters and two series of cluster with only a single atom in +3 but all others in +5 oxidation state: these are the main characteristics of the spectrum.

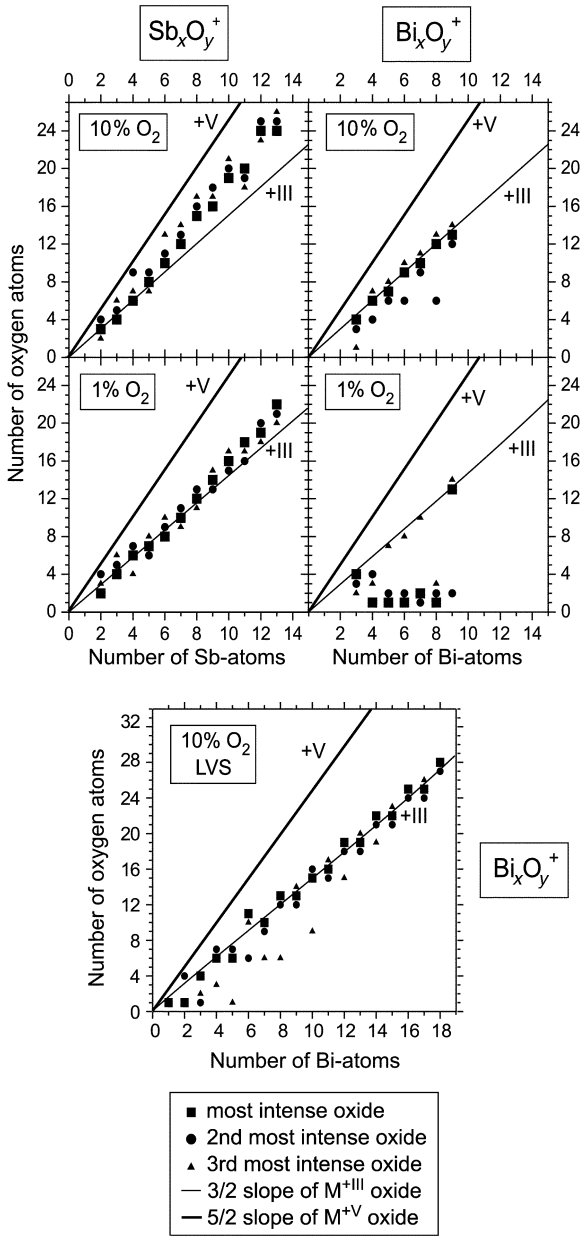

Fig. 8 Correlation diagram for the composition of the cations $M_xO_y^+$ (M = Sb or Bi). The number of O atoms y is plotted against the number of metal atoms x of the three most intense clusters for a defined x. These data are extracted from the respective mass spectra in Figs. 3 and 4 (PACIS) and Fig. 5 (LVS).

are inserted into the clusters' network by changing the coordination of antimony atoms. With one extra oxygen atom, the energetically lowest structures for $n > 2$ contain a central $Sb^{+V}O_4$ group and no oxygen atoms in terminal positions. Oxygen atoms in a terminal position are found however in the case of smaller clusters or for clusters with two excess oxygen atoms. In analogy it is thought that all additional excess oxygen atoms are placed in terminal positions changing the oxidation state of the affected antimony atom from +3 to +5. The structure of the time-of-flight mass spectrum [Fig. 3] shows that the group maxima (5,8 and so forth) are assigned to antimony oxide cluster cations with an intermediate number of antimony atoms in +3 and +5 oxidation states. The oxidation reactions might be kinetically controlled with reaction times too short to produce abundant antimony oxide clusters having all antimony atoms in a +5 state. This change of the mean oxidation number at 10% O_2 is depicted in the correlation diagram [Fig. 8], where the O/Sb ratio converges towards 5/2.

Bismuth oxide cations

The series of bismuth(III) oxide cluster cations $(Bi_2O_3)_n^+$ and $(Bi_2O_3)_nBiO^+$ are similar to the ones reported for the antimony case. Therefore, it is assumed that the overall structural designs and building principles in the series $(M_2O_3)_nMO^+$ and $(M_2O_3)_n^+$ are the same for both of the elements M = Sb or Bi. The structural similarities have been shown at least for the small clusters $Bi_xO_y^+$ (x = 3, 4 and 5) by *ab initio*[12] or DFT[14] calculations. The more noble character of bismuth compared to antimony is expressed in its tendency to form similar oxide distributions only at higher oxygen concentrations than was necessary for antimony. The correlation diagrams for the Bi/O composition express this difference: At low oxygen concentration (1%) incomplete oxidation occurs, while at 10% oxygen bismuth(III) oxide cluster cations dominate. The low intensity or absence of higher oxidised bismuth oxides is certainly due to the relativistic inert pair effect for the $6s^2$ electrons of Bi that leads to a very unstable Bi in the formal oxidation state +V. This observation is in agreement with the general chemical behaviour expected for the bismuth(V) compounds. Nevertheless, higher oxidised bismuth clusters are formed in the molecular beam, but they have been shown for the case of $Bi_3O_5^+$ and for $Bi_4O_7^+$ to contain O–O bonds rather than Bi^{+V}.[14] These calculations also reveal that $Bi_3O_6^+$ contains an ozonide-like O–O–O chain whereas $Bi_4O_8^+$ has a positive formation enthalpy and should not be stable, which is in agreement with our experimental results.

Since the members of the series $(Bi_2O_3)_n^+$ are radical cations missing one valence to an O-atom (or formally, a half O-atom) there is a competition in stability with the clusters containing one additional oxygen atom. This effect leads to similar intensities for the series $(Bi_2O_3)_n^+$ and $(Bi_2O_3)_nO^+$ and is more pronounced in the laser vaporisation mass spectra as discussed later. The competition can be described in terms of the above mentioned scheme of electron counting, showing for the series $(Bi_2O_3)_n^+$ a formal vacancy whereas $(Bi_2O_3)_nO^+$ has an electron surplus with respect to the presupposed oxidation states −2 for O and +3 for Bi.

In addition to the PACIS experiments, a laser vaporisation cluster source has been used to investigate the influence of different formation conditions on the clusters' intensity patterns. In both sources the target material is evaporated as a plasma, which cools down by collisions with seed gas atoms leading to supersaturation and finally cluster formation. But the flow conditions differ characteristically: In the PACIS the clusters are embedded in a short gas pulse while in the laser vaporisation source a continuous gas flow is used at a pressure of about 20 mbar. The resulting differences in aggregation time and collision rates in the channels of the sources as well as different adiabatic expansion cooling could influence the appearance patterns of the clusters. Nevertheless, the measured time-of-flight mass spectra for both sources are in very good agreement, which certainly reflects the important influence of the thermodynamics rather than kinetic effects. Consequently, high cluster intensities of the specified "magic" series represent their special thermodynamical stability.

The laser vaporisation mass spectra [Fig. 5] show clearly the thermodynamically favoured formation of bismuth(III) oxides. For the laser vaporisation source we now discuss in detail the conditions, under which these stoichiometric bismuth oxide clusters have been formed. Bismuth is evaporated in an oxygen containing plasma. At an oxygen concentration of 10% oxide formation and cluster growth is finished at least 65 mm after the position of the laser vaporisation. This has been shown recently for the here used experimental set-up by reactivity measurements.[13] The total length of the applied reaction channel is usually 105 mm. If molecular oxygen is added *via* the reactive gas inlets to the gas flow containing the embedded oxide clusters only a slight depletion

of the entire signal can be found. There are no changes of the relative intensities and under these conditions no additional signals appear. This depicts the special stability of the observed cluster series. Nearly oxygen-free bismuth clusters have been observed, if the molecular oxygen is not mixed to the seed gas but added at the second reactive gas inlet at C2 (see Fig. 2), which is located 65 mm after the laser vaporisation zone and 40 mm before the end of the channel. Traces of oxides can only be detected, if the molecular oxygen is added at the first port at C1 located 30 mm after the vaporisation zone with partial pressures of O_2 more than 2 mbar, corresponding to a concentration of about 10%. These results reveal clearly that the oxidation of bismuth takes place in the plasma in front of or even at the surface of the bismuth target. These suggestions are supported by similar results obtained by laser desorption of solid bismuth(III) oxide[32] or partially oxidised bismuth.[21] The substitution of molecular oxygen by nitrous oxide N_2O with concentrations up to 10% yields no bismuth oxide formation at all neither if the N_2O is premixed in the seed gas nor if it is added at the reactive gas inlets. Also, the Bi/O correlation diagrams [Fig. 8] emphasise the favoured formation of cationic bismuth oxide clusters with average O/Bi ratios of 3/2 corresponding to the stoichiometric +3 oxide.

An additional series of peaks $(Bi_4O_6)Bi_x^+$ ($x = 0$–4), which has not been discussed yet, is remarkable in both cationic bismuth oxide mass spectra (PACIS: Fig. 4B, and LVS: Fig. 5). The clusters $(Bi_4O_6)Bi_x^+$ could be formed by coaggregation of single Bi atoms or small Bi_x clusters and a pre-formed Bi_4O_6 unit. Proceeding on the assumption of a primary formation of Bi_4O_6, which is thermodynamically favoured as discussed above, one could understand the special intensities of this oxide series containing six oxygen atoms. Preliminary structural concepts for this series based on an intact Bi_4O_6 unit have not been supported by DFT calculations.[40] Furthermore, also clusters containing isolated Bi_x units seem to be unstable. However, a favoured structure, for instance of $(Bi_4O_6)Bi_4^+$ consists of a Bi_4O_4 ring bridged with a Bi_4 chain. Such 8-membered rings are already known as important structural elements of antimony oxide clusters.[25] The bismuth atoms in that ring are two- or three-fold coordinated with oxygen, whereas the chain atoms are only singly coordinated. The extent of the ring restricts the length of the chain to four metal atoms.

Bismuth oxide anions

The above-discussed results for the cationic oxide clusters have shown that bismuth adopts preferably the +3 oxidation state. A similar behaviour is expected for the anionic oxides, which should lead to similar magic series for the bismuth oxide anions in comparison with the cations. Starting from a cationic series the corresponding anionic clusters would contain two additional electrons. These two electrons could be contributed by an additional oxygen atom. For example, electron counting would predict the existence of the series $(Bi_2O_3)_nBiO_2^-$ as derived from the magic cationic series $(Bi_2O_3)_nBiO^+$. In fact, this anionic series is a main feature in the mass distribution at 1% O_2 as to be seen in Fig. 6.

This stability prediction based on the electron counting rules can also be applied to the other cationic series $(Bi_2O_3)_n^+$ and $(Bi_2O_3)_nO^+$. Indeed, the expected series $(Bi_2O_3)_nO^-$ and $(Bi_2O_3)_nO_2^-$ are clearly present in the anionic oxide mass spectra. The measured distributions at 1% O_2 consist mainly of the predicted anionic series $(Bi_2O_3)_nBiO_2^-$, $(Bi_2O_3)_nO^-$ and $(Bi_2O_3)_nO_2^-$. In the lower mass range, members of the three anionic series are not necessarily the most intense ones in their group. $Bi_3O_6^-$ and $Bi_5O_9^-$ show higher intensity. Possibly, the extra oxygen atoms in these clusters form peroxide bonds to avoid changing the bismuth oxidation state, but this transition to +5 is not entirely excluded. Despite its instability, oxobismuthates(v) are known in the solid state and used, for example, as a component of some high T_c superconductors.[41] From this point of view $Bi_3O_6^-$ and $Bi_5O_9^-$ could correspond to $(Bi_2^{III}O_3)_nBi^VO_3^-$ ($n = 1$ and 2).

However, the correlation diagram [Fig. 9] exhibits the tendency to form bismuth(III) oxide anions. The compositions are uniformly shifted by one or two O atoms to higher oxygen content in respect to the solid stoichiometric oxide. The shift expresses the extra oxygen, which contributes the additional two electrons in the anionic oxide clusters. For vanadium oxide clusters this effect has been recently reported by Bell *et al.*[9]

Antimony oxide anions

The marked peaks in the mass distribution formed at 1% O_2 [see Fig. 7A] resemble systems containing all metal atoms in +3 oxidation state, which has been discussed earlier exemplary of the bismuth oxide anions. For instance, the prominent clusters $Sb_3O_5^-$ and $Sb_5O_8^-$ belong to $(Sb_2O_3)_nSbO_2^-$, ($n = 1$ and 2), since $Sb_4O_8^-$ and $Sb_6O_{11}^-$ are members of $(Sb_2O_3)_nO_2^-$ ($n = 2$ and 3). The adjoined radical series $(Sb_2O_3)_nO^-$ is represented by $Sb_2O_4^-$ and $Sb_4O_7^-$, which are the maximum peaks in their groups. Additionally, the mass spectra at 1% O_2 contain clusters with lower as well as higher oxygen content in respect to the above mentioned series. At 10% O_2 in the seed gas the low oxidised clusters are vanished completely whereas oxygen rich anions become dominant [Fig. 7 B].

Supposing a possible oxidation state +5 for all antimony atoms the high oxidised series $(Sb_2O_5)_nSbO_3^-$ is predicted to be existent. Observed members of this series are $Sb_3O_8^-$ and $Sb_5O_{13}^-$. But more conspicuous are clusters having one or

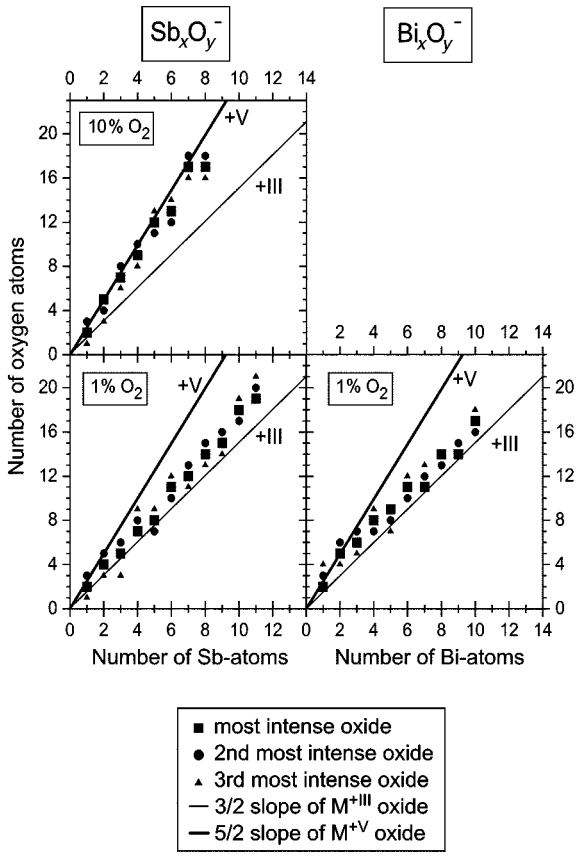

Fig. 9 Correlation diagram for the composition of the anions $M_xO_y^-$ (M = Sb or Bi). These data are extracted from the respective mass spectra in Figs. 6 and 7.

two antimony atoms still in +3 as for instance $Sb_3O_7^-$ and $Sb_5O_{12}^-$, which belong to $(Sb_2O_5)_nSbO_2^-$. Clusters containing an even number of Sb atoms which all adopt the +5 oxidation state, following $(Sb_2O_5)_n^-$, are radicals as discussed for the +3 oxidation state. Again, clusters with an average oxidation number between +3 and +5 for antimony dominate their group. For example, if only one antimony atom turns into +3 the resulting series is $(Sb_2O_5)_n(Sb_2O_4)^-$, prominent elements of this series are $Sb_4O_9^-$ and $Sb_6O_{14}^-$. At 10% O_2, small peaks in the mass spectra can be found, which are beyond the positions of the antimony(V) oxide anions. These oxides carry additional oxygen, which might be peroxidic or weakly adsorbed molecular oxygen.

The correlation diagram in Fig. 9 summarises the formation behaviour of the antimony oxide anions. The trend to form +5 oxides at increasing oxygen concentrations is exhibited in a rising slope of the O/Sb ratio if the oxygen concentration in the seed gas is changed from 1% to 10%. Even the smallest oxide clusters tend to change the oxidation state of at least one antimony atom from +3 to +5.

Summary and conclusion

We have compared systematically the composition of stable cationic and anionic antimony and bismuth oxide clusters. The investigations of mass spectra confirm the possibility of predicting the stability of anionic oxide clusters.

In the Sb/O as well as Bi/O systems, specific thermodynamical stable oxide clusters are preferentially formed at sufficiently high oxygen concentrations. Similarities and differences between the oxide distributions of antimony and bismuth, especially at low oxygen concentrations, are apparent from the presented correlation diagrams. The oxide clusters show magic number behaviour expressed in the following series for the cations $(M_2O_3)_nMO^+$, $(M_2O_3)_n^+$, $(M_2O_3)_nO^+$ and for the anions $(M_2O_3)_nMO_2^-$, $(M_2O_3)_nO^-$, $(M_2O_3)_nO_2^-$, which all contain the metal atoms in a formal +3 oxidation state. Solely for antimony the formation of cluster oxides containing Sb^{+V} becomes favoured, especially at higher oxygen concentrations. This transition in the oxidation state of single antimony atoms in the cluster takes place gradually, as can be seen clearly in the correlation diagram. In particular, the mass spectra of antimony oxide anions reveal series containing Sb^{+V} and a single Sb^{+III} atom, for instance $(Sb_2O_5)_nSbO_2^-$ and $(Sb_2O_5)_n(Sb_2O_4)^-$. In contrast to antimony, bismuth adopts predominantly the +3 oxidation state in the oxides, in agreement with the solid state behaviour.

Moreover, we also studied the influence of different reaction conditions on the formation of antimony and bismuth oxides. The observed "magic" cluster oxide patterns are most likely caused by the thermodynamical stability of the cluster. The thermodynamical preference of such oxide clusters causes similar mass distributions to be obtained even with different cluster sources providing various cluster growth milieus. Further information about thermodynamical values, building blocks and structure of these interesting oxide systems will be deduced from their fragmentational behaviour. We expect a better understanding of these details from our experiments on the dissociation induced by surface collisions.

Acknowledgement

This work has been supported financially by the Fonds der Chemischen Industrie and the Deutsche Forschungsgemeinschaft [Leibniz program Ra 494/9-1]. We are very grateful to Prof. V. Bonacic-Koutecky and Dr M. Bienati for helpful discussions and theoretical support.

References

1 W. A. de Heer, W. D. Knight, M. Y. Chou and M. L. Cohen, *Solid State Phys.*, 1987, **40**, 93.
2 A. W. Castleman, Jr. and K. H. Bowen, Jr., *J. Phys. Chem.*, 1996, **100**, 12911.
3 J. Jortner, *Z. Phys. D; At. Mol. Clusters*, 1992, **24**, 247.
4 S. M. Owen, *Polyhedron*, 1988, **7**, 253.
5 D. M. P. Mingos, T. Slee and L. Zhenyang, *Chem. Rev.*, 1990, **90**, 383.
6 D. C. Parent and S. L. Anderson, *Chem. Rev.*, 1992, **92**, 1541.
7 M. B. Knickelbein, *Annu. Rev. Phys. Chem.*, 1999, **50**, 79.
8 E. F. Fialko, A. V. Kikhtenko, V. B. Goncharov and K. I. Zamaraev, *J. Phys. Chem. A*, 1997, **101**, 8607.
9 R. C. Bell, K. A. Zemski, D. R. Justes and A. W. Castleman, Jr., *J. Chem. Phys.*, 2001, **114**, 798.
10 P. Jackson, J. N. Harvey, D. Schröder and H. Schwarz, *Int. J. Mass Spectrom.*, 2001, **204**, 233.
11 B. D. Leskiw, A. W. Castleman, Jr., C. Ashman and S. N. Khanna, *J. Chem. Phys.*, 2001, **114**, 1165.
12 M. Kinne, A. Heidenreich and K. Rademann, *Angew. Chem.*, 1998, **110**, 2637.
13 A. Fielicke and K. Rademann, *J. Phys. Chem. A*, 2000, **104**, 6979.
14 M. Bienati, V. Bonacic-Koutecky and P. Fantucci, *J. Phys. Chem. A*, 2000, **104**, 6983.
15 B. V. Reddy and P. Jena, *Chem. Phys. Lett.*, 1998, **228**, 253.
16 R. Reinicke, *Z. Elektrochem.*, 1935, **41**, 23.
17 M. J. Buerger and S. B. Hendricks, *J. Phys. Chem.*, 1937, **5**, 600.
18 V. Meyer and C. Meyer, *Ber. Dtsch. Chem. Ges.*, 1879, **12**, 1282.
19 G. C. Hampson and A. J. Stosick, *J. Am. Chem. Soc.*, 1938, **60**, 1814.
20 L. R. Maxwell, S. B. Hendricks and L. S. Deming, *J. Chem. Phys.*, 1937, **5**, 626.
21 M. R. France, J. W. Buchanan, J. C. Robinson, S. H. Pullins, R. B. King, J. L. Tucker and M. A. Duncan, *J. Phys. Chem. A*, 1997, **101**, 6214.
22 M. Kinne, T. M. Bernhardt, B. Kaiser and K. Rademann, *Int. J. Mass Spectrom. Ion Processes*, 1997, **167/168**, 161.
23 M. Kinne, T. M. Bernhardt, B. Kaiser and K. Rademann, *Z. Phys. D: At. Mol. Clusters*, 1997, **40**, 105.
24 B. Kaiser, T. M. Bernhardt, M. Kinne and K. Rademann, *Int. J. Mass Spectrom.*, 1998, **177**, L5.
25 B. Kaiser, T. M. Bernhardt, M. Kinne, K. Rademann and A. Heidenreich, *J. Chem. Phys.*, 1999, **110**, 1437.
26 V. S. Ban and B. E. Knox, *J. Chem. Phys.*, 1970, **52**, 248.
27 N. M. Sammes, G. A. Tompsett, H. Näfe and F. Aldinger, *J. Eur. Ceram. Soc.*, 1999, **19**, 1801.
28 V. A. Maroni and T. G. Spiro, *Inorg. Chem.*, 1968, **7**, 183.
29 B. Sundvall, *Inorg. Chem.*, 1983, **22**, 1906.
30 C. M. Jones, M. D. Burkart and K. H. Whitmire, *J. Chem. Soc., Chem. Commun.*, 1992, 1638.
31 E. Oniyama and P. G. Wahlbeck, *J. Phys. Chem. B*, 1998, **102**, 4418.
32 V. S. Ban and B. E. Knox, *J. Chem. Phys.*, 1970, **52**, 243.
33 M. J. Van Stipdonk, D. R. Justes, R. D. English and E. A. Schweikert, *J. Mass Spectrom.*, 1999, **34**, 677.
34 G. Ganteför, H. R. Siekmann, H. O. Lutz and K. H. Meiwes-Broer, *Chem. Phys. Lett.*, 1990, **165**, 293.
35 H. R. Siekmann, C. Lüder, J. Faermann, H. O. Lutz and K. H. Meiwes-Broer, *Z. Phys. D: At. Mol. Clusters*, 1991, **20**, 417.
36 T. M. Bernhardt, Doctoral thesis, Humboldt-Universität zu Berlin, 1997.
37 W. C. Wiley and I. H. McLaren, *Rev. Sci. Instrum.*, 1955, **26**, 1150.
38 N. R. Daly, *Rev. Sci. Instrum.*, 1960, **31**, 264.
39 D. Bahat, O. Cheshnovski, U. Even, N. Lavie and Y. Magen, *J. Phys. Chem.*, 1987, **91**, 2460.
40 M. Bienati and V. Bonacic-Koutecky, personal communication, 2000.
41 L. F. Mattheiss, E. M. Gyorgy and J. D. W. Johnson, *Phys. Rev. B: Condens. Matter*, 1988, **37**, 3745.